

The flow field in the sunspot canopy

R. Rezaei¹, R. Schlichenmaier¹, C.A.R. Beck¹, and L.R. Bellot Rubio^{1,2}

¹ Kiepenheuer-Institut für Sonnenphysik, Schöneckstr. 6, 79104 Freiburg, Germany

² Instituto de Astrofísica de Andalucía (CSIC), Apdo. 3004, 18080 Granada, Spain

Received 10 March 2006/Accepted 28 March 2006

ABSTRACT

Aims. We investigate the flow field in the sunspot canopy using simultaneous Stokes vector spectropolarimetry of three sunspots ($\theta = 27^\circ, 50^\circ, 75^\circ$) and their surroundings in visible (630.15 and 630.25 nm) and near infrared (1564.8 and 1565.2 nm) neutral iron lines.

Methods. To calibrate the Doppler shifts, we compare an absolute velocity calibration using the telluric O₂-line at 630.20 nm and a relative velocity calibration using the Doppler shift of Stokes *V* profiles in the umbra under the assumption that the umbra is at rest. Both methods yield the same result within the calibration uncertainties ($\sim 150 \text{ m s}^{-1}$). We study the radial dependence of Stokes *V* profiles in the directions of disk center and limb side.

Results. Maps of Stokes *V* profile shifts, polarity, amplitude asymmetry, field strength and magnetic field azimuth provide strong evidence for the presence of a magnetic canopy and for the existence of a radial outflow in the canopy.

Conclusions. Our findings indicate that the Evershed flow does not cease abruptly at the white-light spot boundary, but that at least a part of the penumbral Evershed flow continues into the magnetic canopy.

Key words. Sun: photosphere – Sun: sunspots – Sun: magnetic fields

1. Introduction

From the pioneering work of Evershed (1909), we know that there is a flow field in the sunspot penumbra, which leads to a line shift and line asymmetry. For sunspots outside the disk center, it manifests in blue shifted spectral lines in the center side and red shifted spectral lines in the limb side. The penumbral fine structure has a close relation with the Evershed flow. It is generally accepted that the flow channels are more horizontal than the background field (Solanki 2003). Because spectropolarimetric data has lower spatial resolution than narrow band magnetograms, many questions regarding both the Evershed flow and the fine structure of the penumbra have remained (e.g. Solanki 2003; Bellot Rubio 2004). There are also controversial arguments about the continuation of the Evershed flow outside the sunspot.

Brekke & Maltby (1963) studied horizontal variations of the Evershed flow. Investigating 2500 sunspot spectra, they reported that at the outer penumbral boundary “the velocity falls abruptly to zero”. Wiehr et al. (1986) observed a sharp decrease of the Evershed effect and magnetic field at the visible boundary of sunspots. Using only Stokes *I* spectra, they argued that line-core shifts and line asymmetries are “strongly” limited to the continuum boundary of sunspots. Wiehr & Balthasar (1989), Schröter et al. (1989) and Title et al. (1993) confirmed the result of Brekke & Maltby (1963). Wiehr (1996) renewed his argument that the Stokes *I* profile asymmetries of Ni I

543.6 nm ($g = 0.5$) and Fe I 543.5 nm ($g = 0$) “disappear” within less than one arcsec from the penumbral border. Hirzberger & Kneer (2001) observed two sunspots at heliocentric angles of 31° and 20° ; they reported a sharp decrease of the Evershed flow (intensity profile asymmetry) at the penumbral boundary, using Stokes *I* of the non-magnetic Fe I 557.6 nm and Fe I 709.0 nm lines.

In contrast, Sheeley (1972) stated that there is a horizontal flow in the plage-free photosphere surrounding sunspots with an average velocity of $\sim 0.5 - 1 \text{ km s}^{-1}$. Küveler & Wiehr (1985) did not find a sharp change in the Evershed flow at the penumbral boundary. Dialektis et al. (1985), Alissandrakis et al. (1988), and Börner & Kneer (1992) confirmed this result. Giovanelli & Jones (1982) reported magnetogram observations of diffuse, almost horizontal magnetic field surrounding two spots at moderate heliocentric angles. Taking Stokes *V* and *I* profiles of the $1.56 \mu\text{m}$ iron lines for two limb spots, Solanki, Montavon, & Livingston (1994) found that the magnetic field of sunspots continues beyond the visible boundary and forms an extensive canopy above a non-magnetic layer. These authors computed the canopy base height and reported that around 10 % of the Evershed flow continues into the magnetic canopy. Rimmele (1995a, b) also found no sharp boundary in time-averaged velocity maps of a sunspot close to the disk center. After observing the Fe I 557.6 nm line with a narrow-band filtergraph, he obtained different velocities at different bisector levels which do not decrease abruptly at the

sunspot boundary. Solanki et al. (1999) repeated their claims about continuation of the Evershed flow by considering V and I signals of the $1.56\ \mu\text{m}$ iron lines for another sunspot close to the limb ($\mu = \cos\theta = 0.22$). Computing the amplitude of the azimuthal velocity variation, Schlichenmaier & Schmidt (2000) did not find a drop of the line-core velocity of Fe II 542.5 nm at the penumbral boundary. Therefore, this long standing disagreement about continuation/termination of the flow field at the sunspot boundary was intensified.

However, it is important to note that none of the mentioned authors observed the full Stokes parameters of the target spots. Moreover, a majority of them only used Stokes I profiles, which suffer from stray light contamination. Here, we present simultaneous spatially co-aligned full Stokes spectropolarimetric observations of three sunspots and their surroundings in visible (630.15 and 630.25 nm) and near infrared (1564.8 and 1565.2 nm) neutral iron lines. These co-temporal and co-spatial observations of the full Stokes vector provide valuable information not only about magnetic field strength in the canopy, but also about the field orientation as emphasized by Solanki et al. (1994). The near-IR neutral iron lines mostly form deep in the atmosphere, while the contribution function of the visible iron lines at 630 nm peaks in higher layers (Cabrera Solana et al. 2005). As these lines form in different atmospheric layers and have large Zeeman sensitivities, they provide a powerful tool to study the properties of the canopy, its flow field and vertical structure.

Considering the fact that the Stokes profiles of Q , U , and V are formed only in a magnetized atmosphere, this data set contains information regarding the extension of the magnetic canopy and the Evershed flow outside the white-light sunspot boundary. In sections 2 and 3, we explain our observations and data reduction in detail. In section 4, the spatial variation of the flow field is investigated using two independent methods. Conclusions and comparisons are discussed in Sect. 5.

2. Observations

Three isolated sunspots (cf. Fig. 1) were observed at the German Vacuum Tower Telescope (VTT) in Tenerife, August 2003. Simultaneous co-aligned spectropolarimetric data with the Tenerife Infrared Polarimeter (TIP) and the Polarimetric Littrow Spectrograph (POLIS) were recorded. The TIP (Collados 1999; Martínez Pillet et al. 1999) observed full Stokes profiles of the infrared iron lines at 1564.8 nm ($g = 3$) and 1565.2 nm ($g = 1.53$). The visible neutral iron lines at 630.15 nm, 630.25 nm, and Ti 630.38 nm were observed with the POLIS (Schmidt et al. 2003; Beck et al. 2005a).

For the spots 1 and 3, the scanning step-size was 0.35 arcsec, while for spot 2 it was 0.4 arcsec. Spatial sampling of the TIP maps along the slit was 0.35 arcsec. For the POLIS, the spatial sampling along the slit was 0.15 arcsec (Beck et al. 2005a). To improve the signal-to-noise ratio and to have a comparable spatial resolution as in the infrared data, we bin the data along the slit by a factor of 3. The pixel size of these new maps along the slit is 0.44 arcsec. The spectral sampling of 2.97 pm for TIP and 1.49 pm for POLIS leads to a velocity dispersion of $570\ \text{m s}^{-1}$ and $700\ \text{m s}^{-1}$ per pixel, respectively. Seeing

Table 1. Properties of the observed sunspots. θ is the heliocentric angle. The last column is the scanning step-size in arcsec.

Spot No.	Date	Active Region	θ (°)	step-size
1	09/08/2003	10430	27	0.35
2	03/08/2003	10425	50	0.40
3	08/08/2003	10421	75	0.35

conditions during the observations were good and stable. We used the Correlation Tracker System (Schmidt & Kentischer 1995; Ballesteros et al. 1996) to compensate for image motion. We estimate the spatial resolution to be about 1.0 arcsec for the spots 1 and 2 and 1.5 arcsec for the spot 3. The duration of the observations for each sunspot was around 10 minutes.

The spectropolarimetric data of both TIP and POLIS have been corrected for instrumental effects and telescope polarization with the procedures described in Collados (1999; Martínez Pillet et al. 1999) for the TIP and Beck et al. (2005a, b) for the POLIS. Remaining cross-talk in our data sets is of the order of $10^{-3} I_c$. Table 1 summarizes the characteristics of the three observations. The spot closest to the limb was at $\theta = 75$ deg.

3. Data analysis

In this section, we explain the data reduction and present our definition for the sunspot boundary. Then we investigate two independent methods of velocity calibration. Finally, we extract vector magnetic field parameters.

3.1. Pre-processing

We use a continuum intensity threshold to define umbral data points and their mean position, the umbral center. After that, we draw a radial line from the umbral center in azimuthal directions (in 0.5° steps). The point at which this line crosses the penumbral white-light boundary defines the sunspot border and radius in this direction. The continuum threshold which are used at the penumbral border are 0.8 and $0.9 I_c$ for the visible and infrared data respectively. These crossing points define a closed path (contour) around each sunspot (cf. Fig. 1, left column).

All polarization signals, $Q(\lambda)$, $U(\lambda)$, $V(\lambda)$, and the total linear polarization profiles, $L(\lambda) = \sqrt{Q(\lambda)^2 + U(\lambda)^2}$, are normalized by the local continuum intensity, I_c , for each pixel, i.e., $V(\lambda) \equiv V(\lambda)/I_c$. The rms noise level of Stokes parameters in the continuum is $\sigma = 3 - 5 \times 10^{-4} I_c$ for the infrared lines and $\sigma = 1.5 \times 10^{-3} I_c$ for the visible lines. Only pixels with V signals greater than 5σ for TIP (3σ for POLIS) are included in the analysis. Positions and amplitudes of the profile extrema in all Stokes parameters are obtained by fitting a parabola to each lobe.

For the POLIS data, we apply a correction along the slit before calibrating the velocity. In this direction, there is a curvature in the profiles due to the small focal length of the spectrograph. For each scan step, a third order polynomial is fitted to positions of the 630.20 nm telluric line-cores along the slit. All profiles in that scan step are shifted with the resulting curve.

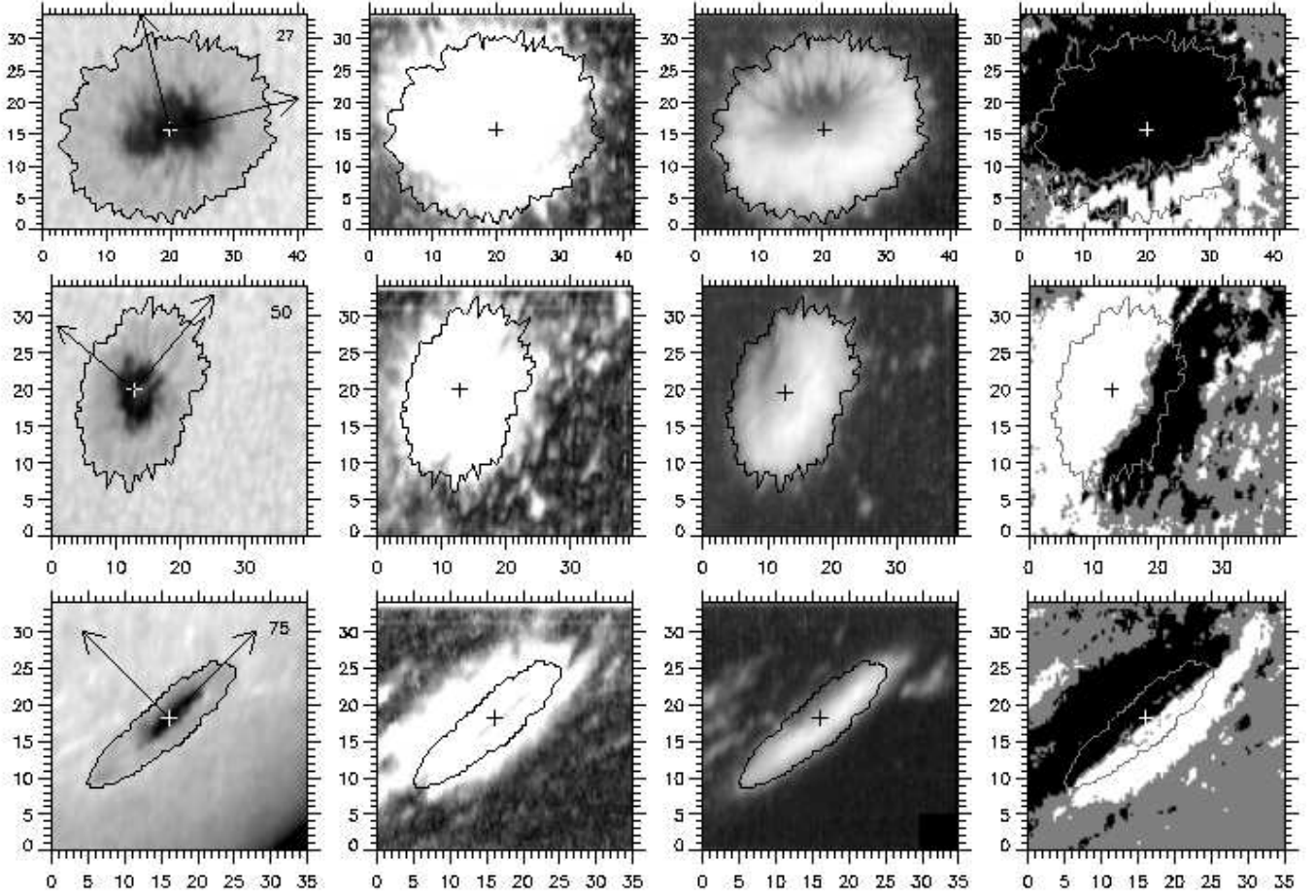


Fig. 1. From left to right: continuum intensity maps of the sunspots, integrated circular polarization ($\int |V(\lambda)| d\lambda$), the integrated linear polarization signal ($L_t = \int L(\lambda) d\lambda$), and polarity in FeI 1564.8 nm line. From top to bottom: spot 1, spot 2, and spot 3. Axis labels are spatial dimensions in arcsec. The numbers on the upper-right corners are the heliocentric angles of the spots. In the white-light maps, the left arrows show the disk center directions. Note that the magnetic field clearly extends over the white-light boundary along the line connecting sunspot to the disk center in the V maps and perpendicular to this line in L_t maps.

This correction amounts at most to ~ 4 (spectral) pixels shift between upper most and lower most spatial pixels. Final maps of the line-core velocity of the telluric line are quite uniform with a small dispersion (standard deviation) in the umbral region, e.g. around 0.11 pixel ($\equiv 77 \text{ m s}^{-1}$) for the spot 1. Using this telluric rest-frame, we calibrate Stokes V and I shifts.

3.2. Velocity calibration

We consider two different calibration methods. The first method is based on Stokes V profiles of the umbra. Assuming that the umbra is at rest, we select quite antisymmetric Stokes V profiles. The Stokes V profile is expected to be strictly antisymmetric with respect to its zero-crossing wavelength, if no velocity gradients with height is present and if LTE applies (Auer & Heasley 1978; Landi Degl’Innocenti & Landolfi 1983). Hence, the mean position of these profiles is assumed to define a *rest-frame*. To confirm the assumption of the umbra at rest, we perform an absolute velocity calibration using the telluric lines in the POLIS data. At the end of this section, we

compare the two calibration methods. Results are completely consistent and differences are less than the calibration error.

3.2.1. Velocity calibration using Stokes V profiles of the umbra

We attribute a relative amplitude asymmetry, δa , to each $V(\lambda)$ profile. It is defined as the asymmetry between the amplitudes of the two lobes of Stokes V by:

$$\delta a = \frac{a_b - a_r}{a_b + a_r},$$

where a_b and a_r are the absolute amplitudes of blue and red lobes, respectively. The center of each $V(\lambda)$ profile is defined as the midway between its maximum and minimum. This quantity is better than deriving the zero-crossing by a linear regression, because it is less affected by magneto-optical effects. First, all umbral profiles with an amplitude asymmetry lower than a threshold are selected, which defines a class corresponding to a row in Table 2. Then, the relative velocity of each selected profile with respect to the mean value of the class (reference point)

Table 2. From top to bottom: spot 1, 2, and 3. The first column is the maximum amplitude asymmetry in each class. d_1 (d_2) shows the velocity dispersion of the selected umbral profiles in infrared (visible) lines in each row. % IR (vis) gives the number of umbral profiles in percent of all umbral pixels with δa less than the threshold. The fourth and the last columns are difference of velocity reference point of each class relative to the final result ($|\delta a| \leq 0.05$). The last row gives number of total umbral profiles. Velocities are in m s^{-1} .

max. $ \delta a $	d_1	% IR	ref: IR	d_2	% vis	ref: vis
0.10	143	100	-6	112	100	0
0.07	143	98	-6	112	99	0
0.05	137	96	-	112	98	-
0.03	143	66	12	112	91	0
0.02	137	41	18	112	74	0
0.01	125	20	41	119	42	0
0.10	108	99	0	155	77	14
0.07	108	96	6	148	61	7
0.05	108	71	-	155	50	-
0.03	114	40	6	183	28	-7
0.02	114	25	12	211	17	-14
0.01	120	11	41	-	-	-
0.10	205	79	18	268	91	14
0.07	216	65	12	268	83	0
0.05	176	52	-	282	75	-
0.03	170	41	-24	275	59	-35
0.02	114	31	-41	268	42	-35
0.01	80	16	-59	247	23	-28
N_{tot} 1/2/3		649/321/153			434/263/135	

is determined. So each class has a velocity dispersion around its mean value which is defined to be zero. The velocity dispersions for different classes are similar (d_1 and d_2 in Table 2). These are the main uncertainties in the Stokes V velocity calibration. The difference between reference point of each class and the $|\delta a| \leq 0.05$ class is given in Table 2 (fourth and last columns). We select the mean position of a set of quite anti-symmetric umbral profiles with $|\delta a| \leq 0.05$ as the sunspot rest-frame, which is a compromise between low amplitude asymmetry and good statistics (Table 2).

In spot 3, the magnetic neutral line lies inside the umbra, because the spot is close to the limb. Therefore, inside the sunspot the longitudinal component of the magnetic field along the line of sight is weaker than the transverse component. Hence, the Stokes V profiles are not reliable for the calibration purpose. For this reason, we use the linear polarization components instead. We decided to use the profile center of the Stokes Q (position of the π component) in this case and use the amplitude asymmetry of the σ components in Q as a measure of the line antisymmetry. The dispersion of the velocity reference points in the selected umbral pixels (spot 3) is slightly higher than for spots 1 and 2 (Table 2). We estimate a maximum calibration error for the spot 3 of $\sim 250 \text{ m s}^{-1}$. This does not affect our conclusions, because velocity values in spot 3 are larger than in spots 1 and 2. From the velocity dispersions in each class (d_1 and d_2), we estimate that we achieve a precision of

Table 3. Wavelengths of the spectral lines in the POLIS data. The laboratory wavelengths are from Higgs (1960, 1962). The rest value includes the gravitational redshift ($\Delta\lambda = 2.12 \times 10^{-6}\lambda$).

	Laboratory (Å)	rest (Å)	air (Å)
Fe I	6301.4990	6301.5124	-
O ₂	-	-	6302.0005
Fe I	6302.4920	6302.5054	-
O ₂	-	-	6302.7629
Ti I	6303.750	6303.763	-

$\pm 150 \text{ m s}^{-1}$ for the spots 1 and 2 and $\pm 250 \text{ m s}^{-1}$ for the spot 3 in the TIP and POLIS data, respectively¹.

3.2.2. Absolute velocity calibration

Using the telluric lines in the POLIS data, it is possible to perform an absolute velocity calibration for these data sets (Schmidt & Balthasar 1994; Martínez Pillet et al. 1997; Sigwarth et al. 1999). We use the 630.20 nm line, because it is less influenced by the solar iron lines in the umbra than the O₂-line at 630.27 nm. We only correct line-core positions for the curvature of the spectrograph as explained in Sect. 3.1. Then, the radial velocity between the observatory and the sunspot is determined. We use the values of Balthasar et al. (1986) for the sunspot angular rotation ([14.551, -2.87], cf. their Eq. (1)) to compute the radial velocity components: the earth rotation, the earth orbital motion and the solar rotation. Total radial velocities for the spots 1, 2, and 3 (sum of the three components) are 0.253, 0.862 and 1.327 km s^{-1} , respectively. These values take into account the line of sight component of the solar rotation, which amounts to 0.918, 1.438, and 1.971 km s^{-1} . Gravitational correction is also considered for all solar lines (Table 3). Here, the rest-frame for each resolution element is the position of the telluric line plus a constant shift which includes proper correction for the radial velocity. In other words, there is a reference point in each resolution element different from the others.

Source of errors Apart from the precision of the solar center and sunspot positions, the main challenge is to determine the exact sunspot angular rotation. Angular rotation of sunspots depends on the age and probably the phase of the solar cycle. It is also affected by the sunspot proper motion. So, the radial velocity values remain uncertain within $\sim \pm 100 \text{ m s}^{-1}$. Moreover, there are some errors in positioning during the observations. For example, 5 arcsec error in the solar longitude creates an error of $\sim 15 \text{ m s}^{-1}$ in the radial velocity (depending on the position). Pixel by pixel variation due to different time and slit positions cause a maximum error of $\sim 10 \text{ m s}^{-1}$ between the first and the last scan steps. Therefore, we conclude that for the absolute velocity calibration the precision is $\pm 150 \text{ m s}^{-1}$.

Oscillations in the photospheric level of the umbra may induce errors in the Stokes V calibration. However observations imply that such fluctuations are small. Martínez Pillet et al.

¹ Our convention is that positive values correspond to redshift.

Table 4. Mean values and dispersions of the umbral velocities for the 630.25 nm iron line in km s^{-1} . The last column shows uncertainties in the Stokes V and absolute calibrations for the spots 1 and 2. These values for the spot 3 are 0.211 and 0.282 km s^{-1} respectively. It confirms our principal assumption that the umbra is at rest (within our calibration error).

spot 1	Stokes I	Stokes V	error
Stokes V calib	0.085 ± 0.242	-0.023 ± 0.059	0.112
absolute calib	-0.135 ± 0.258	-0.258 ± 0.060	0.176
spot 2			
Stokes V calib	-0.158 ± 0.143	-0.038 ± 0.088	0.176
absolute calib	-0.168 ± 0.135	-0.044 ± 0.072	0.211

(1997), for example, studied a large sample of active regions and reported an umbral velocity of 65 m s^{-1} due to umbral oscillations. Balthasar & Schmidt (1994) also investigated five minute oscillations in the umbra and reported an amplitude of 90 m s^{-1} (rms).

3.2.3. Comparison of the two calibration methods

In order to check the assumption that the umbra is at rest, we compare the two calibration methods. Subtracting the corresponding velocity maps for Fe I 630.25 nm yields a difference map that show low amplitude variations, definitely less than the calibration uncertainties. It is important to note that we used a constant velocity reference point in the first method for the whole image, while in the absolute calibration we used different reference points (one for each spatial pixel). To compare the absolute calibration with the first method, we define a mean reference point for the absolute calibration, the corrected telluric line position in the umbra.

Comparing Stokes V and absolute calibrations, there are small differences between them and also small dispersions in each one: Table 4 lists the mean umbral velocities for the *whole umbra* for the Fe I 630.25 nm line obtained from both methods. The average Stokes V umbral velocities with absolute calibration confirm that our basic assumption, taking the umbra at rest, is correct. Average line–core velocities are also less than our calibration errors. Their tendency for a blueshift is probably due to stray light contamination from the quiet sun. However, in the Stokes V absolute calibration there is a tendency for a blueshift because the average velocities of the whole umbra include umbral dots and periphery points. These lead to the weak blueshifts in the umbra, comparable to our calibration precision. There are reports of strong upflows in the umbra of preceding spots in bipolar pairs (e.g. Sigwarth 2000); however all three spots were isolated. Our results do not exclude that there are some oscillations in the umbra, but the amplitudes should be less than our precision limit of $\pm 150 \text{ m s}^{-1}$ (as reported by, e.g. Lites et al. 1998; Bellot Rubio et al. 2000a).

The absolute calibration confirms our first method based on the Stokes V profiles of the umbra. Therefore, we can confidently use this method where an absolute calibration is not possible like for the TIP data.

3.3. Magnetic field parameters

To investigate the flow field in the canopy, we calculate line parameters for all *regular* $V(\lambda)$ profiles, i.e. profiles which show two clear lobes. The quantities derived are positions and amplitudes of the peaks, area and amplitude asymmetries, and the magnetic field strength. We also analyze $Q(\lambda)$, $U(\lambda)$, and $L(\lambda)$ of the TIP data in order to have a measure for the inclination and azimuth of the magnetic field. We construct maps of field strength, azimuth, amplitude asymmetry of Stokes V , and Stokes V velocities (Fig. 2). Comparing the second and third columns of Fig. 2, it is clear that the magnetic neutral line in the visible is shifted outward with respect to the infrared line. The field strength is calculated using the Stokes V splitting of the 1564.8 nm line. The line is a Zeeman triplet which is in the strong field limit for $B > 0.03 \text{ T}$; so we can use the distance between the σ component and the profile center as a measure of the magnetic field strength (e.g. Stix 2002) by:

$$\Delta\lambda = 4.67 \times 10^{-18} \lambda^2 g_{\text{eff}} B$$

where g_{eff} is the effective Landé factor, $\Delta\lambda$ and λ are in nm, and B is in tesla. This is not an exact method, especially for weak fields. So these estimates are upper limits for the weak magnetic field of the canopy. This method fails along the magnetic neutral line. Maps on the left column of Fig. 2 show the field strength.

Considering the fact that these Stokes profiles are formed in the weak field limit in the canopy, one may use the ratio of the σ components of the linear and circular polarization to approximate the magnetic field inclination and azimuth (e.g. Stix 2002; Solanki 1993)

$$\frac{V}{\sqrt{Q^2 + U^2}} \sim \frac{\cos \gamma}{\sin^2 \gamma} \quad \text{and} \quad \frac{U}{Q} \sim \tan(2\chi)$$

where γ is the inclination with respect to the line of sight and χ is the azimuth with respect to the celestial N–S direction. In the weak field limit, these ratios are independent of the field strength. Computing field orientation in this way is not as accurate as an inversion. However, it is sufficient for our purpose to check whether or not the field geometry in the canopy follows the same pattern as in the spot. The azimuth maps in Fig. 2 (right column) show the same pattern inside and outside the spot in the canopy. Thus, the canopy can be distinguished in these maps from the separate magnetic elements, which show different azimuth and field strength.

Because linear polarization signals are usually weaker than the circular polarization, it is not possible to compute the field azimuth for all pixels with a reasonable V signal. Moreover, the field strength in the canopy is much smaller than in the spot. For this reason, we have smaller coverage in the azimuth maps, which come from linear polarization signals, with respect to other maps which are based on V signals (Fig. 2). Pattern of various parameters outside the spot in Fig. 2 show a smooth change at the spot boundary. In other words, the magnetic field strength and orientation, and the flow field do not change *abruptly* at the sunspot white–light boundary.

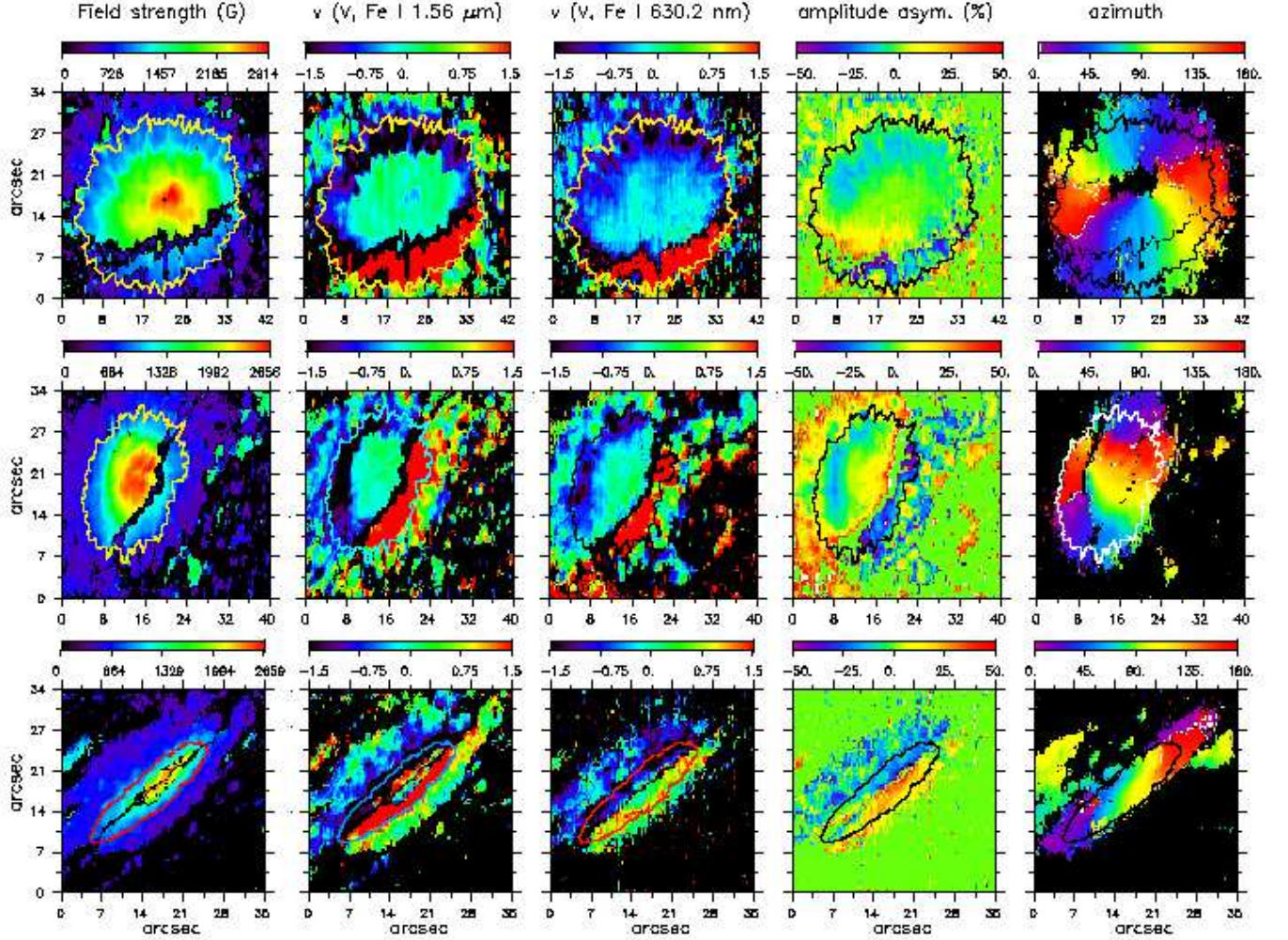


Fig. 2. From left to right: field strength, B , in Gauss (10^{-4} T); Stokes V velocity in 1564.8 nm in km s^{-1} ; Stokes V velocity in 630.25 nm in km s^{-1} ; Stokes V amplitude asymmetry in 630.25 nm (%); magnetic field azimuth in degree. From top to bottom: spot 1, spot 2, and spot 3. As it is clear in the Stokes V amplitude asymmetry of spot 3, there are significant amplitude asymmetries in the umbra due to the presence of the magnetic neutral line. Also note the usually larger velocities outside the penumbral boundary in the visible (630.25 nm) than infrared (1564.8 nm) line. Magnetic field strength and azimuth obviously indicate that the magnetic field of sunspots continue outside the white-light boundary with the same orientation. Separate magnetic elements may be easily distinguished in these maps.

4. Radial outflow in the canopy

In this section, we define the magnetic canopy to be distinguished from the isolated magnetic elements. We investigate Stokes V profiles in radial cuts, both on the limb and center sides. Box-car averaging in radial directions is another method to investigate the canopy. Finally, we study the canopy extension in our sunspots.

4.1. Canopy definition and isolated magnetic elements

The maximum distance at which there is a magnetic field along with a flow (with consistent *sign and gradient*) varies for different spots. We attribute a pixel in a radial cut to the sunspot canopy, if it demonstrates all the properties below:

1. It has the same magnetic polarity and velocity sign as the preceding pixel closer to the spot boundary.
2. It shows the same inclination and azimuth patterns as the preceding pixel closer to the spot boundary.
3. Both the absolute values of the velocity and magnetic field strength decrease with respect to the preceding pixel or remain constant.

The right column of Fig. 1 illustrates the polarity maps. It is clear that close to each spot, there is a unipolar-connected region that we attribute to the canopy. But as we go outward, some isolated magnetic elements appear with either different polarities or velocity signs. Therefore, the *sign and gradient* of velocity at some of these points do not show a monotonic behavior. These isolated magnetic elements are seen in various

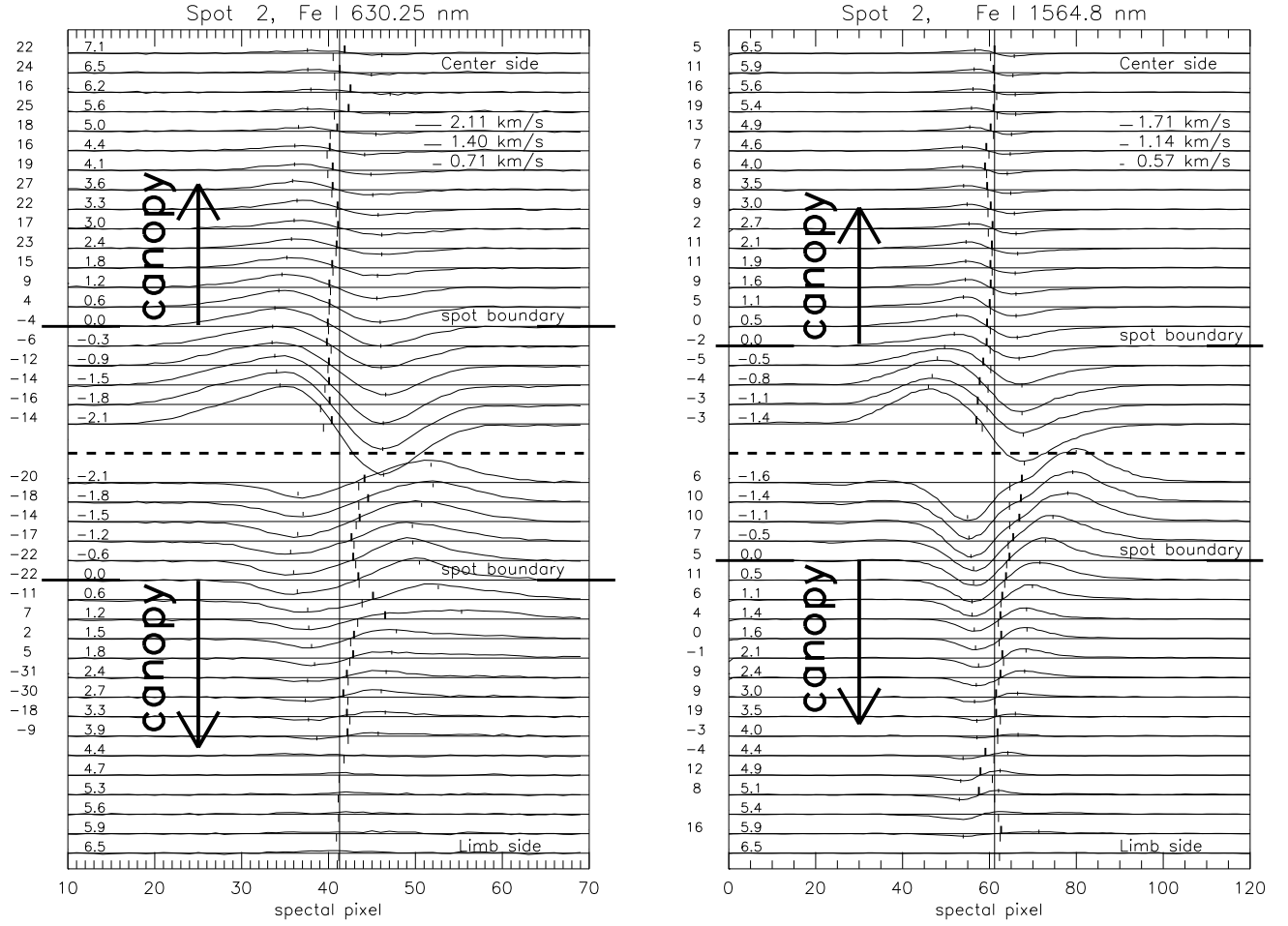


Fig. 3. $V(\lambda)$ profiles in a radial cut in the axis of symmetry of spot 2 in the POLIS (left) and TIP (right) data. Thin tick marks are positions of the max/min of the two lobes. Thick tick marks above the horizontal line are the profile centers of Stokes V . Thin tick marks below the horizontal line show the corresponding Stokes I (line-core) velocity. Vertical solid line is the velocity reference point based on the umbral calibration. Numbers on the left column inside the diagram are distance of each profile from the spot boundary in arcsec. The left hand side numbers outside the diagram are the amplitude asymmetries in percent. Note the usually larger amplitude asymmetries in the visible data. The thick dashed horizontal lines show the discontinuity in the diagram and separate the limb and center side. Three small lines indicate the amounts of required shifts for some velocities. Sunspot boundaries in the limb and center side are indicated.

maps of Figs. 1, 2 (e.g. at $x = 36$ and $y = 24$ arcsec in the spot 2).

4.2. Stokes V profiles in radial cuts

Fig. 3 shows Stokes V profiles in a radial cut in the limb and center side directions (axis of symmetry) for the spot 2 in the TIP and POLIS data. In this figure, the Stokes V velocity smoothly decreases outward *without any abrupt change* at the sunspot boundary. The sign and gradient of the velocities remain constant at first, but start to change in the outer parts. Note the very broad red lobes in the limb side in the visible data, while the corresponding profiles in the infrared data are not so much affected (but still are broader than the blue lobes). It may be due to the presence of magnetic structures high in the atmosphere such that they cannot significantly affect the 1.56

μm lines. Stokes V velocities of these broad profiles have to be considered with caution. Around 4 arcsec from the penumbral boundary in the center side, there is a jump in velocity in both lines. Further out on this side, the velocity changes sign. This indicates that these points cannot be attributed to the sunspot canopy. Another interesting feature is a separate magnetic element ~ 5 arcsec from the spot boundary on the limb side in the infrared line. Within two arcsec, redshift of the profile center converts to blueshift and then changes to redshift. Also note the amplitude of the $V(\lambda)$ profile, which decreases and then increases. The same is true for the magnetic field strength (Stokes V splitting). The amplitude asymmetry of each profile is also indicated in Fig. 3. There are large amplitude asymmetries which may be due to gradients or jumps in the magnetic field and/or velocity (e.g. Bellot Rubio et al. 2000b).

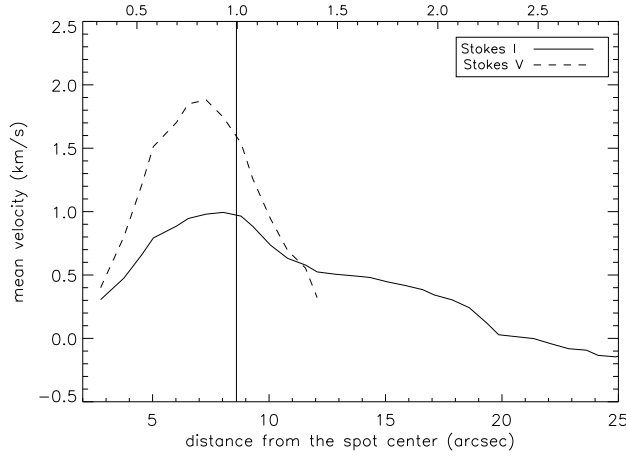


Fig. 4. The solid line is the line-core velocity and the dashed line is the Stokes V velocity of Fe I 1564.8 nm in the limb side of the spot 2. The vertical line is the penumbral boundary (± 0.2 arcsec for differences in neighbor pixels). Inside the spot, V and I Stokes velocities follow each other, while they show different behaviors outside the spot. Upper x-axis is the distance from the penumbral boundary in units of sunspot radius. The averaging box is 17×17 pixels to cover granules and intergranular lanes.

4.3. Box-car averages of the flow and field parameters in the sunspot symmetry axis

Comparison of the line-core and Stokes V velocities plays an important role in distinguishing the radial outflow in the canopy and the moat flow. We average velocities in small square boxes along the symmetry axis of the sunspots. We have large coverage outside the spot in the limb side of the spot 2; so we study this case in detail. Inside the penumbra, the line-core velocities are smaller than the Stokes V velocities, having a similar radial dependence (cf. Fig. 4). Outside the spot, the curves of line-core and Stokes V velocities intersect each other. Thus, a few arcsec outside the penumbral boundary, the value of the Stokes V velocity in the visible/infrared is less than the corresponding Stokes I velocity. The intersection points for the infrared lines are slightly closer to the sunspots than visible lines. The range of the velocities in the canopy is $\sim 0.5 - 2.0 \text{ km s}^{-1}$. High velocity patches are rare. Roughly speaking, a velocity of 1.0 km s^{-1} is common in the canopy of all the three spots. This is far from the average values for the line-core velocities. These are around $0.6 - 0.7 \text{ km s}^{-1}$ close to the sunspots, reaching $\sim -0.2 \text{ km s}^{-1}$ (the typical values for the convective blueshift) at the boundary of the moat cell. At these distances, there is no uniformly connected canopy as described above. Magnetic fields of these regions are governed by the plage activity and isolated magnetic elements floating in the sunspot moat.

The contribution function of the iron lines at 630 nm peaks in higher layers relative to the lines at $1.56 \mu\text{m}$. Visible lines form in larger geometrical extents than the infrared lines. In addition, Stokes V profiles form exclusively in the magnetic part of the atmosphere. The fact that we usually observe larger Stokes V velocities in the visible than in the infrared in the

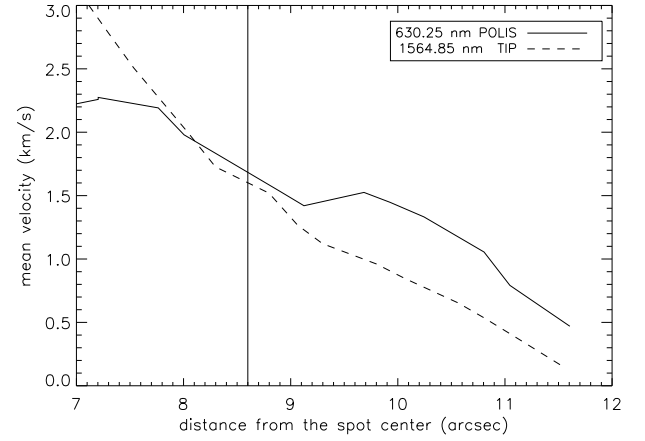


Fig. 5. This plot shows the radial variation on Stokes V velocities on the limb side of the spot 2. The solid line is the visible Fe I 630.25 nm Stokes V velocity and the dashed line is the same for the near IR Fe I 1564.8 nm. The vertical line is the penumbral boundary (± 0.2 arcsec for differences in neighbor pixels). Inside the sunspot, the TIP data show larger velocities while outside the spot, the POLIS data show larger values. The averaging box is 5×5 pixels in this diagram.

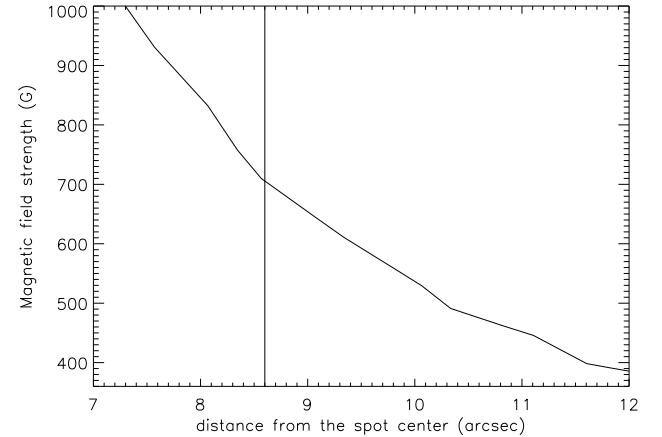


Fig. 6. Same as Fig. 5 for the magnetic field strength in the TIP data.

canopy (Figs. 2, 5) implies that there is a flow in the magnetic part of the atmosphere which affects the visible lines more than the infrared lines. Observations by Balthasar et al. (1996) of the moat flow in non-magnetic lines resulted in low amplitude smooth velocity field ($\sim 0.5 \text{ km s}^{-1}$), similar to velocities we find in the Stokes I data. Beside this, the spatial extension of the moat flow is much more than what we observe in the Stokes V maps. There are also significant amplitude asymmetries in the sunspot canopy (Figs. 2, 3) which indicate that there are gradients or jumps in the velocity field. Therefore, the line-core velocity is comparable with the moat flow velocity in non-magnetic lines while the Stokes V velocity is not a reasonable proxy for the moat flow. Hence, we attribute line-core velocity to the moat flow and Stokes V velocity to the canopy outflow.

We find average amplitude asymmetries in the canopy profiles of $\sim 10\%$. These values are less than the maximum amplitude asymmetry, which peaks in the middle/outer penumbra (Schlichenmaier & Collados 2002). Amplitude asymmetries of the canopy in spot 2 are given in Fig. 3. The profile asymmetry is one of the typical properties of the Evershed flow, which we observe in the canopy radial outflow. It is different from the amplitude asymmetry in plage and network which changes from one pixel to the next one. We usually observe gradually changing amplitude asymmetries in nearby pixels (Fig. 3).

The magnetic field strength decreases smoothly outside the spot (Fig. 6). There is no sharp change at the penumbral boundary or within 1 arcsec. The lobe separation in the Stokes V profiles of the canopy is a measure of the minimum magnetic field. The smallest Stokes V splitting observed are ~ 0.03 T. As we go outward and leave the uniform-connected canopy with coherent flow field, disturbances in the observed $V(\lambda)$ profiles increase. At some point, Stokes V splitting increases while the amplitude decreases (Fig. 3, limb side, Fe I 1564.8 nm line, profile at 5.9 arcsec).

The average canopy extensions of 1.2, 1.35, and 1.6 (± 0.05) penumbral radii for the spots 1, 2, and 3 depend almost linearly on the cosine of the heliocentric angle. We observe similar canopy extensions in the visible and infrared lines. All the three sunspots were observed with the same setup and exposure time. It may be possible to trace larger canopies close to the disk center with longer exposure times, and hence higher signal-to-noise ratios.

5. Conclusion

We investigate the flow and magnetic field in the immediate surroundings of three sunspots using spectropolarimetric data observed simultaneously at the VTT in two spectral regions around Fe I 1564.8 nm and around Fe I 630.2 nm, with TIP and POLIS, respectively. The existence of a radial outflow in the sunspot canopy is a matter of strong debate. Here, we provide strong evidence for the existence of the canopy, and for the existence of a radial outflow in the canopy by analyzing Stokes profiles.

To this end it is essential to properly calibrate the velocity. We use two different calibration methods. The first one is based on the assumption that the most antisymmetric profiles in the umbra reflect locations at rest. The second is an absolute calibration which uses the telluric line in the vicinity of Fe I 630.2 nm, taking into account the relative motions between the telescope and the surface of the sun. Both methods are consistent, which implies that antisymmetric V profiles in the umbra represent a rest-frame.

Evidence for the existence of a canopy surrounding all three sunspots at various heliocentric angles is presented:

- (1) The polarization signal extends outside the sunspot white-light boundary up to 1.2, 1.35, and 1.6 penumbral radii for spots at $\mu = 0.89, 0.64$, and 0.26 respectively.
- (2) We find that velocities and the estimated magnetic field strength vary smoothly across the penumbral boundary. There is no abrupt change within one arcsec, which corresponds to our spatial resolution.

- (3) The field azimuth and polarity in the canopy follow the spot pattern.

- (4) Velocities determined from Doppler shifts of Stokes V show a radial outflow in the surroundings of sunspots. The same is true for line-core velocities from Stokes I , but as argued in Sect. 4.3, the latter is related to the moat flow.

- (5) Significant amplitude asymmetries of Stokes V exist almost everywhere in the surroundings of sunspots, indicating depth gradients or discontinuities in the flow velocity.

All our findings are consistent with a magnetic canopy surrounding sunspots, which exhibits a discontinuity (magnetopause) rising with radial distance from the spot. Moreover, our findings indicate that the radial outflow in the canopy is an extension of the penumbral Evershed flow. The decreasing V -velocity with radial distance from the spot is consistent with a rising canopy base, i.e. with a magnetopause which rises outwards from the spot. Line-core velocities of Stokes I persist outwards in the surroundings of sunspots and are therefore attributed to the moat flow. As one would expect, the canopy extension increases with heliocentric angle, and even at a small heliocentric angle of 27° the canopy extension is at least 3 arcsec, much more than the spatial resolution. Therefore, we conclude that at least a part of the penumbral Evershed flow continues in a magnetic canopy that surrounds sunspots.

Acknowledgements. We wish to thank Wolfgang Schmidt, Hubertus Wöhl, and Dirk Soltau for useful discussions. Daniel Cabrera Solana (IAA) kindly provided the routine for the radial velocity calculation.

References

- Alissandrakis, C.E., Dialetis, D., Mein, P. et al., 1988, A&A 201, 339
- Ballesteros, E., Collados, M. & Bonet, J.A., 1996, A&AS 115, 353
- Balthasar, H. & Schmidt, W., 1994, A&A 290, 649
- Balthasar, H., Vázquez, M. & Wöhl, H., 1986, A&A 155, 87
- Balthasar, H., Schleicher, H., Bendlin, C. & Volkmer, R., 1996, A&A 315, 603
- Beck, C., Schmidt, W., Kentischer, T. & Elmore, D., 2005a, A&A 437, 1159
- Beck, C., Schlichenmaier, R., Bellot Rubio, L.R. & Kentischer, T., 2005b, A&A, 443, 1047
- Bellot Rubio, L.R., 2004, Sunspots as seen in polarized light, Reviews in Modern Astronomy, 17, Ed. R.E. Scielicke, Wiley
- Bellot Rubio, L.R., Collados, M., Ruiz Cobo, B. et al., 2000a, ApJ 534, 989
- Bellot Rubio, L.R., Ruiz Cobo, B. & Collados, M., 2000b, ApJ 535, 489
- Bellot Rubio, L.R., Balthasar, H., Collados, M. & Schlichenmaier, R., 2003, A&A 403, L47
- Börner, P. & Kneer, F., 1992, A&A 255, 307
- Brekke, K. & Maltby, P., 1963, Ann. d'Astrophys. 26, 383
- Cabrera Solana, D., Bellot Rubio, L.R., & del Toro Iniesta, J.C., 2005, A&A 439, 687
- Collados, M., 1999, in ASP Conf. Ser. 184, Thirds Advances in Solar Physics Euroconference: Magnetic Field and Oscillation, 3
- Dialetis, D., Mein, P., & Alissandrakis, C.E., 1985, A&A 147, 93
- Evershed, J., 1909, MNRAS, 69, 454
- Giovanelli, R.G. & Jones, H.P., 1982, Solar Phys 79, 267
- Higgs, L.A., 1960, MNRAS, 121, 421
- Higgs, L.A., 1962, MNRAS, 124, 51
- Hirzberger, J. & Kneer, F., 2001 A&A 378, 1078

- Küveler, G. & Wiehr, E., 1985, A&A 142, 205
- Landi Degl'Innocenti, E. & Landolfi, M., 1983, Solar Phys 87, 221
- Leka, K.D., & Steiner, O., 2001, ApJ 552, 354
- Lites, B.W., Thomas, J.H., Bogdan, T.J. et al., 1998, ApJ 497, 464
- Martínez Pillet, V., Lites, W. & Skumanich, A., 1997, ApJ 474, 810
- Martínez Pillet, V., Collados, M., Sanchez Almeida, J. et al., 1999, in ASP Conf. Ser. 183, High Resolution Solar Physics: Theory, Observation, and Techniques, 264
- Rimmele, R.T., 1995a, ApJ 445, 511
- Rimmele, R.T., 1995b, A&A 298, 260
- Schlichenmaier, R. & Collados, M., 2002, A&A 381, 668
- Schlichenmaier, R. & Schmidt, W., 2000, A&A 358, 1122
- Schmidt, W. & Balthasar, H., 1994, A&A 283, 241
- Schmidt, W. & Kentischer, T., 1995, A&AS 113, 363
- Schmidt, W., Beck, C., Kentischer, T. et al., 2003, AN 324, 300
- Schröter, E.H., Kentischer, T., & Münzer, H., 1989, in High Spatial Resolution Solar Observations, O. van der Lühse (Ed.), National Solar Obs., Sunspot, NM, p. 299
- Sheeley N.R., Jr., 1972, Solar Phys 25, 98
- Sigwarth, M., 2000, Rev Mod Ast, 13, 45
- Sigwarth, M., Balasubramaniam, K.S., Knölker, M. & Schmidt, W., 1999, A&A 349, 941
- Solanki, S.K., 1993, Space Sci Rev, 63, 1
- Solanki, S.K., 2003, A&AR 11, 153
- Solanki, S.K., Montavon, C.A.P., & Livingston, W., 1994, A&A 283, 221
- Solanki, S.K., Finsterle, W., Rüedi, I. & Livingston, W., 1999, A&A 347, L27
- Steiner, O., 2000, Solar Phys 196, 245
- Stix, M., 2002, The Sun: An Introduction, Springer
- Title, A.M., Frank, Z.A., Shine, R.A. et al., 1993, ApJ 403, 780
- Wiehr, E., 1996, A&A 309, L4
- Wiehr, E. & Balthasar, H., 1989, A&A 208, 303
- Wiehr, E., Stellmacher, G., Knölker, M. & Grosser, H., 1986, A&A 155, 402